Temperature dependence of the acoustic-mode vibrational anharmonicity of quartz from 243 to 393 K

Q. Wang, G. A. Saunders, and E. F. Lambson
School of Physics, University of Bath, Bath BA2 7AY, United Kingdom

P. Tschaufeser and S. C. Parker
School of Chemistry, University of Bath, Bath BA2 7AY, United Kingdom

B. J. James
GEC Hirst Research Centre, East Lane, Wembley, Middlesex HA9 7PP, United Kingdom
(Received 24 September 1991)

Measurements made of the effects of hydrostatic pressure on ultrasonic wave velocities have been used to obtain the hydrostatic-pressure derivatives of the six independent second-order elastic constants (SOEC's) and the bulk modulus of very-high-purity quartz crystals in the temperature range 243–393 K. The results, which quantify the nonlinear properties of quartz, show that $(\partial C_{IJ}/\partial P)_{T,P=0}$ depend markedly upon temperature (contrary to their previous usage in technological applications as temperature-independent quantities), some to the extent of having a maximum or minimum in their values, in this technologically important temperature range. The compression estimated at very high pressures using the Murnaghan equation of state is in reasonable agreement with experimental data. A theoretical calculation of the six elastic-stiffness-tensor components and their hydrostatic-pressure derivatives has also been made by atomistic simulation techniques with the short-range interaction between Si and O ions represented by the Buckingham potential. A comparison between the calculated and experimental results shows good agreement for the SOEC's themselves (the second derivatives of the potential energy with respect to the strain) and also reasonable accord for the $(\partial C_{IJ}/\partial P)_{T,P=0}$, which are the combinations of the third derivatives of the potential energy with respect to the strain. That the hydrostatic-pressure derivatives $(\partial C_{14}/\partial P)_{T,P=0}$ and $(\partial C_{66}/\partial P)_{T,P=0}$ have negative signs has interesting ramifications concerning the nature of the α-β displacive phase transition of quartz. A detailed description of the vibrational anharmonicity of the long-wavelength acoustic modes is given in terms of their Grüneisen parameters in the quasiharmonic approximation. Certain shear and quasishear acoustic modes have negative acoustic-mode Grüneisen parameters, thus accounting for the negative value of the thermal-expansion-tensor component α_{33} at low temperatures. The mean acoustic-mode Grüneisen parameter γ_H^{el} in the long-wavelength limit decreases markedly in the temperature range 243–330 K due to the temperature dependences of the hydrostatic-pressure dependences $(\partial C_{IJ}/\partial P)_{T,P=0}$ of the elastic-stiffness-tensor components.

I. INTRODUCTION

To investigate the nonlinear behavior of very-high-purity quartz (VHPQ), the hydrostatic-pressure derivatives of its second-order elastic-stiffness-tensor components (SOEC's) have been measured in the temperature range 243–393 K, in which quartz devices are usually operated. As a result of the considerable technological significance of the elastic stiffnesses C_{IJ} and their temperature coefficients as input data in resonator and oscillator device designs, they have been measured by many authors using a wide variety of techniques.[1–6] In the case of very-high-purity quartz, James[6] has reported the first set of all six SOEC's and their temperature coefficients in the temperature range 213–393 K. However a linear description of quartz device effects is not adequate for the design and usage of the next generation of resonators, oscillators, and frequency control devices. Knowledge of higher-order elastic coefficients is needed to quantify the nonlinear effects responsible for most frequency instabilities. In addition, a design requirement of high-precision quartz resonators, oscillators, and surface-acoustic-wave devices is to incorporate in the analysis, by means of the SOEC's and third-order elastic constants (TOEC's), nonlinear effects on resonance frequencies, such as the amplitude-frequency effect, intermodulation of the resonance frequency, and coupling between different vibration modes. The available data for higher-order elastic constants do not provide a sufficiently comprehensive description of the nonlinear acoustic behavior of quartz over the range of temperature in which quartz devices are usually operated. Third- and fourth-order elastic constant combinations corresponding to some longitudinal modes have been reported.[7,8] The hydrostatic-pressure dependences of the six independent second-order elastic constants of quartz at 298 and 77 K and all of the fourteen third-order elastic constants (TOEC's) at 298 K have been measured[9,10] using the ultrasonic pulse superposition technique. However, these data do not define the temperature dependences of either the pressure deriva-

tives of the SOEC's or the TOEC's. The present contribution is to provide complex sets of values of hydrostatic-pressure derivatives $(\partial C_{IJ}/\partial P)_{T,P=0}$ of the second-order elastic-stiffness-tensor components for VHPQ in the temperature range 243–393 K. To enhance understanding of the physical origin and nature of the elastic and nonlinear properties of quartz, a theoretical calculation of the SOEC's and their pressure derivatives $(\partial C_{IJ}/\partial P)_{T,P=0}$ has been performed using the atomistic simulation method. By comparing the calculated results with the measured data, a rigorous test of the potential used in the simulation can be made.

The pressure dependence of the SOEC's is one of the consequences of vibrational anharmonicity of the acoustic modes in the long-wavelength limit in crystals. This vibrational anharmonicity is related to nonlinear interatomic forces with respect to atomic displacements. Thus, knowledge of the pressure derivatives of the SOEC's is essential to any investigation of the nonlinear elastic properties and the acoustic-mode vibrational anharmonicity of crystals. Measurement of the effect of hydrostatic pressure on the velocity of ultrasonic modes propagated in a crystal is the most accurate way of determining these pressure derivatives. When combined with the dependence of ultrasonic wave velocity upon uniaxial stress, such results lead to the eventual evaluation of the TOEC's, which quantify the cubic terms in the strain Hamiltonian. However, for many practical purposes the hydrostatic-pressure derivatives of the elastic-stiffness-tensor components suffice. For example they establish the pressure dependence of the bulk modulus and hence, the equation of state. They also can be used to evaluate the acoustic-mode Grüneisen parameters, which measure the effect of hydrostatic pressure on the frequency of the long-wavelength acoustic modes and also the contribution of these acoustic phonons to the thermal expansion. The temperature dependence of the hydrostatic mode Grüneisen parameters has been determined by using the measured $(\partial C_{IJ}/\partial P)_{T,P=0}$. This clarifies the variation of the contribution of the acoustic-wave modes to the thermal expansion of quartz as a function of temperature.

II. EXPERIMENTAL PROCEDURE

The samples used were two blocks of the recently developed very-high-purity quartz (VHPQ) prepared by the Hirst Research Centre of the GEC company at Wembley, Middlesex. Three orthogonal reference faces on each block were orientated using an x-ray goniometer. One block was right-handed and was cut with its axes along the X, Y, and Z crystalline axes, respectively. The other was left-handed and was cut with its axes along a direction at 45° between the $+Z$ and $+Y$ crystallographic axes, 45° between the $+Z$ and $-Y$ crystallographic axes, and along the X axis, respectively. The sample faces were polished optically parallel; all faces were flatter than a quarter wavelength of 633-nm light. On the right-handed XYZ block the worst face misorientation was about 25 arc sec and the worst parallelism approximately one fringe. On the left-handed rotated block at 45° from $+Y$ to $+Z$, the misorientation of the rotated Y' axis was $-2\frac{48}{60}$ arc min and the face misorientation of the work faces was -33 arc sec. The parallelism of the working faces was close to a zero fringe. Having such accurately prepared samples reduces the error from nonparallelism and misorientation to the extent that it can be ignored.

Ultrasonic pulse transit times were measured as a function of pressure and temperature using the ultrasonic pulse echo overlap technique,[11] which is particularly well suited to determination of small changes in velocity. X- and Y-cut quartz transducers with a diameter of 6 mm were employed for generating the 10 MHz longitudinal and shear wave pulses, respectively. Acoustic coupling to make a thin, uniform transducer-sample bond to ensure an exponentially decaying echo train was achieved using either Dow resin 276-V9 or Du Pont thick film conductor composition as the bonding material. The former provided good acoustic energy coupling for longitudinal wave insertion throughout the temperature range (243–393 K) over which measurements were required but not for shear waves above 313 K when it was not viscous enough. Use of the Du Pont bonding agent formulated for higher temperature usage overcame this problem. The procedure employed for transducer-specimen coupling with the Du Pont agent was: (1) to attach the transducer with Du Pont couplant onto the sample work face, (2) bake at 353–373 K for 8–12 h, (3) cool down naturally to room temperature.

Hydrostatic pressures up to about 2×10^8 Pa were applied in a piston- and-cylinder apparatus constructed from EN26 nickel alloy carbon steel. The pressure transmission fluid was Dow Corning 200/1000cs silicone fluid, which can operate in a temperature range of 243–450 K. Pressure was measured using a precalibrated manganin resistance gauge.[12]

Possible sources of error in the ultrasonic measurements include a time delay due to the phase shift induced by the bonding material estimated using the approach developed by McSkimin[13] as about 0.02% in wave velocity and corrected for. Multiple internal reflections within a transducer can lead to distortion of the pulse envelope and to a time lag of the center of the reflected pulse relative to a signal reflected from the surface of the transducer;[14] a correction has been applied using Kittinger's method.[15] An estimation of the error caused by the diffraction field of the transducer, obtained using Papadakis' analysis,[16] shows that in a threefold (Z) axis direction in quartz, it is about twice for longitudinal wave velocity measurements than for shear waves, but both are less than 1% and have been taken into account. Application of pressure alters the transducer resonant frequency; it is necessary to make a correction for the transducer phase shift due to this effect.[17] The corrections have been incorporated in the computational analysis involved in calculating the pressure derivatives of the elastic constants. Errors in the other parameters, such as those of pressure, temperature, sample dimensions, and density incurred in the measurements are included in the quoted deviations of the data. Temperature induced changes in sample dimensions and density have been corrected for using thermal-expansion coefficients for synthetic stan-

dard grade quartz[6] because those of VHPQ are unavailable.

To circumvent the necessary calculation of the change in crystal dimensions incurred by application of pressure, the experimental data have been transformed into the "natural velocity" W (Ref. 18), which is defined by the equation

$$W=2l_0f \ . \tag{1}$$

Here l_0 is the transit length of the wave and f is the measured frequency of wave round trips in a sample. The advantage of the natural velocity approach is that $(\rho_0W^2)'_{P=0}$ is directly related to the initial slope and intercept of the measured frequency versus the pressure curve of ultrasonic measurements:

$$(\rho_0W^2)'_{P=0}=2\rho_0v_0^2f'/f_0 \ , \tag{2}$$

where f' is the pressure derivative of the measured frequency.

III. DETERMINATION OF THE HYDROSTATIC-PRESSURE DERIVATIVES OF THE ELASTIC-STIFFNESS-TENSOR COMPONENTS

The elastic-stiffness-tensor components of VHPQ have been measured[6] with high precision as a function of temperature and the results need not be duplicated here. However, the set obtained at room temperature is given in Table I where a comparison (discussed in Sec. IV) is made with results calculated theoretically using atomistic simulation. Concerning the central objective of measurement of the pressure derivatives of the elastic stiffnesses, one important feature is that the sign of $C_{14}^{S,E}$ is confirmed as being positive as reported from several previous studies[19–21,6] rather than negative.[10] The tensor component $C_{14}^{S,E}$ of both standard synthetic quartz and VHPQ remains positive in the temperature range 213–393 K.[6]

In the calculations of the pressure derivatives of the SOEC's, it is necessary to distinguish between the effective $C_{ijkm}^{\rm eff}$ and thermodynamic $C_{ijkm}^{S,E}$ elastic constants as defined by Thurston.[22] The superscripts eff, S,E indicate the effective elastic constants and the thermodynamic adiabatic elastic constants in zero electric field, respectively. These quantities are related by

$$C_{ijkm}^{\rm eff}=\tilde{P}(\delta_{ij}\delta_{km}-\delta_{im}\delta_{jk}-\delta_{ik}\delta_{jm})+\frac{\tilde{\rho}}{\rho_0}\frac{\partial X_i}{\partial a_p}\frac{\partial X_j}{\partial a_q}\frac{\partial X_k}{\partial a_r}\frac{\partial X_m}{\partial a_s}C_{ijkm}^{S,E} \ . \tag{3}$$

Here X_i are the coordinates of a particle in the initial stressed state and a_i are the coordinates in the strain-free state. At zero pressure the effective SOEC's tensors and the thermodynamic SOEC's tensors are equal: we can use $C_{jrks}^{S,E}$ to indicate the effective elastic constants at atmospheric pressure.

For piezoelectric crystals the SOEC's tensors $C_{jrks}^{S,E}$ are coupled with the second-order piezoelectric coefficient tensors e_{njr} as

$$C_{jrks}^{st}=C_{jrks}^{S,E}+\frac{e_{njr}N_ne_{lks}N_l}{\varepsilon_{nl}N_nN_l} \ , \tag{4}$$

where the tensors C_{jrks}^{st} are called the "stiffened" elastic coefficients and N_i are the direction cosines of the mode propagation direction.

The hydrostatic-pressure derivatives of the thermodynamic stiffened elastic constants at zero pressure can be defined as

$$B_{jrks}^{st}\equiv\left[\frac{\partial C_{jrks}^{st}}{\partial P}\right]_T=\left[\frac{\partial C_{jrks}^{S,E}}{\partial P}\right]_T+\left[\partial\left[\frac{e_{njr}N_ne_{lks}N_l}{\varepsilon_{nl}N_nN_l}\right]\Big/\partial P\right]_T=B_{jrks}+\left[\partial\left[\frac{e_{njr}N_ne_{lks}N_l}{\varepsilon_{nl}N_nN_l}\right]\Big/\partial P\right]_T \ , \tag{5}$$

TABLE I. Comparison between the theoretical values of C_{IJ} and the bulk modulus B of α-quartz determined at 0 and 300 K using the ASM model and those measured experimentally for VHPQ at 298 K. Pa.

T (K)	C_{11} (10^{10} Pa)	C_{12} (10^{10} Pa)	C_{13} (10^{10} Pa)	C_{66} (10^{10} Pa)
0	8.940	1.030	1.701	3.955
300	8.844	0.518	1.249	4.163
298	8.487±0.002	0.535±0.002	1.215±0.003	3.976±0.002
T (K)	C_{14} (10^{10} Pa)	C_{33} (10^{10} Pa)	C_{44} (10^{10} Pa)	B (10^{10} Pa)
0	1.678	11.218	5.062	4.218
300	1.811	10.206	4.953	3.770
298	1.768±0.003	10.555±0.001	5.781±0.001	3.651±0.003

where

$$B_{jrks}=\left[\frac{\partial C^{S,E}_{jrks}}{\partial P}\right]_T . \tag{6}$$

Thus pressure derivatives can be related to the measured ultrasonic frequency data, using a similar approach to that given for nonpiezoelectric crystals,[22]

$$2\rho_0\nu_0^2 f'/f_0=(\rho_0 W^2)'_{P=0}$$
$$=-1-U^0_j U^0_k(2\rho_0\nu_0^2 s^T_{jkqq}-N_r N_s B^{st}_{jrks}) . \tag{7}$$

Expressions for

$$F=U^0_j U^0_k s^T_{jkqq} \tag{8}$$

and

$$B=U^0_j U^0_k N_r N_s B^{st}_{jrks} \tag{9}$$

for the modes measured here for α-quartz are given in Table II. The pressure derivatives of the effective stiffened elastic constants at $P=0$ can be related to the thermodynamic stiffened elastic constants by

$$\left[\frac{\partial C^{\text{eff},st}_{ijkm}}{\partial P}\right]_{P=0}=\delta_{ij}\delta_{km}-\delta_{im}\delta_{jk}-\delta_{ik}\delta_{jm}+B^{st}_{ijkm}$$
$$+\chi^T C^{S,E}_{ijkm}-C^{S,E}_{pjkm}s^{T,E}_{ttip}-C^{S,E}_{iqkm}s^{T,E}_{ttjq}$$
$$-C^{S,E}_{ijrm}s^{T,E}_{ttkr}-C^{S,E}_{iiks}s^{T,E}_{ttms} . \tag{10}$$

Thurston[23] has worked out the differences between the B_{jrks} and $(\partial C^{\text{eff}}_{jrks}/\partial P)_T$ for crystal symmetries other than monoclinic and triclinic without considering piezoelectric effects. The expressions appropriate to α-quartz are given, in matrix notation, in Table III. The method used here is first to calculate the B^{st}_{jrks} from the measured f'/f_0, next to determine B_{jrks}; then the derivatives with respect to pressure $(\partial C^{\text{eff}}_{jrks}/\partial P)_{T,P=0}$ in the zero pressure limit of the effective elastic constants are evaluated employing the relations in Table III. For convenience we will henceforth denote the pressure derivatives of the effective SOEC's as $(\partial C_{IJ}/\partial P)_{T,P=0}$ with the SOEC's in matrix form.

The hydrostatic-pressure derivatives of the natural velocity $(1/W_0)(\partial W/\partial P)_{P=0}$ of the modes given in Table II have been measured at selected temperatures and the pressure derivatives of the effective $(\partial C_{IJ}/\partial P)_{T,P=0}$ and thermodynamic (B_{IJ}) SOEC's have been evaluated. The wave velocities and their pressure derivatives in the zero pressure limit have been obtained by a least-squares fit to the measured data. A comparison of the experimental values obtained for $(1/W_0)(\partial W/\partial P)_{P=0}$ with the data of McSkimin, Andreatch, and Thurston[10] at 298 K is given in Table IV. For several modes there is reasonable agreement with the earlier data obtained on, presumably at that time, natural quartz single crystals (of unquoted purity). The higher-order elastic-stiffness behavior of a piezoelectric crystal, such as quartz, would be expected to be sensitive to crystal purity and perfection. Substantial differences are found between the

TABLE II. The parameters F and B corresponding to the ultrasonic modes measured for the α-quartz structure. The mode numbers are the same as those used in Ref. 9. The direction cosines of the particle displacement of certain wave modes determined at 298 K are given at the bottom.

Mode	N_1	N_2	N_3	U_1	U_2	U_3	F	B
1	1	0	0	1	0	0	s_1	$B_{11}+\left[\frac{\partial e_1}{\partial P}\right]_T$
2	1	0	0	0	β_1	β_2	$\beta_1^2 s_1+\beta_2^2 s_3$	$\beta_1^2 B_{66}+2\beta_1\beta_2 B_{14}+\beta_2^2 B_{44}$
5	0	1	0	0	γ_2	γ_2	$\gamma_2^2 s_1+\gamma_2^2 s_3$	$\gamma_1^2 B_{11}-2\gamma_1\gamma_2 B_{14}+\gamma_2^2 B_{44}$
6	0	1	0	1	0	0	s_1	$B_{66}+\left[\frac{\partial e_1}{\partial P}\right]_T$
7	0	0	1	0	0	1	s_3	B_{33}
9	0	1	0	0	0	1	s_1	B_{44}
10	0	$1/\sqrt{2}$	$1/\sqrt{2}$	0	θ_1	θ_2	$\theta_1^2 s_1+\theta_2^2 s_3$	$\theta_1^2 B_{11}+(1+2\theta_1\theta_2)B_{44}+2\theta_1\theta_2^2 B_{13}$ $-2(\theta_1^2+\theta_1\theta_2)B_{14}+\theta_2^2 B_{33}/2$
12	0	$-1/\sqrt{2}$	$1/\sqrt{2}$	1	0	0	s_1	$(B_{44}+B_{66})/2-2B_{14}+\left[\frac{\partial e_2}{\partial P}\right]_T$

β_1	β_2	γ_1	γ_2	θ_1	θ_2
0.8529	−0.5221	0.4428	0.8966	0.5137	0.8580

TABLE III. The analytical differences between the pressure derivatives of the effective and thermodynamic SOEC's for the α-quartz structure.

$$(\partial C_{11}^{\text{eff}}/\partial P)_{P=0}-B_{11}=-1+(s_3-2s_1)C_{11}^{S,E}$$
$$(\partial C_{12}^{\text{eff}}/\partial P)_{P=0}-B_{12}=1+(s_3-2s_1)C_{12}^{S,E}$$
$$(\partial C_{13}^{\text{eff}}/\partial P)_{P=0}-B_{13}=1-s_3C_{13}^{S,E}$$
$$(\partial C_{14}^{\text{eff}}/\partial P)_{P=0}-B_{14}=-s_1C_{14}^{S,E}$$
$$(\partial C_{33}^{\text{eff}}/\partial P)_{P=0}-B_{33}=-1+(2s_1-3s_3)C_{33}^{S,E}$$
$$(\partial C_{44}^{\text{eff}}/\partial P)_{P=0}-B_{44}=-1-s_3C_{44}^{S,E}$$
$$(\partial C_{66}^{\text{eff}}/\partial P)_{P=0}-B_{66}=-1+(s_3-2s_1)C_{66}^{S,E}$$

$(1/W_0)(\partial W/\partial P)_{P=0}$ values for mode 1, mode 5, and mode 10 obtained for the two different types of quartz. The hydrostatic-pressure derivatives of the six independent effective SOEC's $(\partial C_{IJ}/\partial P)_{T,P=0}$, calculated from the measured $(1/W_0)(\partial W/\partial P)_{P=0}$, are listed in Table V as a function of temperature. The derivatives $(\partial C_{11}/\partial P)_{T,P=0}$, $(\partial C_{12}/\partial P)_{T,P=0}$, $(\partial C_{13}/\partial P)_{T,P=0}$, and $(\partial C_{66}/\partial P)_{T,P=0}$ include piezoelectric contributions and values with and without these contributions are given in Table V(a); the piezoelectric contributions are considerable. For comparison, the values of the $(\partial C_{IJ}/\partial P)_{T,P=0}$ at 298 K given by McSkimin, Andreatch, and Thurston[10] are also listed in Table V.

Since some modes include a piezoelectric contribution, while others do not (Table II) the pressure dependence measurements can be used to estimate the pressure derivatives of the parameters $e_1=e_{11}^2/\varepsilon_{11}^{\eta}$ and $e_2=(e_{14}-e_{11})^2/2(\varepsilon_{11}^{\eta}+\varepsilon_{33}^{\eta})$, results are given as a function of temperature in Table V(b). The value obtained for $(\partial e_1/\partial P)_{T,P=0}$ at 298 K is larger than that quoted by McSkimin, Andreatch, and Thurston.[10] The values of the pressure derivatives $(\partial C_{IJ}/\partial P)_{T,P=0}$ obtained at 298 K, which have not been adjusted for piezoelectric contributions, are in reasonable agreement with the $(\partial C_{IJ}/\partial P)_{T,P=0}$ given by McSkimin, Andreatch, and Thurston;[10] exceptions being $(\partial C_{13}/\partial P)_{T,P=0}$ and $(\partial C_{14}/\partial P)_{T,P=0}$, which are not related simply to measured velocities but have to be calculated from sequences of sums and differences of squares. A notable difference is that $(\partial C_{14}/\partial P)_{T,P=0}$ is found to be negative, although a positive value was given by McSkimin, Andreatch, and Thurston.[10] This stems directly from the different signs of the elastic constant $C_{14}^{S,E}$ used in the calculation; McSkimin[2] gives $C_{14}^{S,E}$ as -1.904×10^{10} N/m^2 but in the hand convention[24] used we obtain a positive value ($+1.768\pm0.003\times10^{10}$ N/m^2) (Table I) as do other workers.[6,19–21] The positive sign is retained in the temperature range 243–393 K. The pressure derivative of the adiabatic bulk modulus $(\partial B/\partial P)_{T,P=0}$ with the piezoelectric contribution abstracted is given in Table V(b) as a function of temperature; $(\partial B/\partial P)_{T,P=0}$ at 298 K is in reasonable agreement with that determined previously.[10]

The experimental results show that the pressure derivatives $(\partial C_{IJ}/\partial P)_{T,P=0}$ of the SOEC's (Table V) and of the bulk modulus $(\partial B/\partial P)_{T,P=0}$ [Table V(b)] are markedly dependent upon temperature. Each of the derivatives $(\partial C_{11}/\partial P)_{T,P=0}$, $(\partial C_{66}/\partial P)_{T,P=0}$, and $(\partial C_{14}/\partial P)_{T,P=0}$ (after removal of the piezoelectric contribution) show a minimum value at about 283 K. These minima are a direct consequence of a maximum in the measured value of $(1/W_0)(\partial W/\partial P)_{P=0}$ for mode 5, which plays an important role in these derivatives. Quite different behavior with temperature is shown by $(\partial C_{11}/\partial P)_{T,P=0}$ and $(\partial C_{66}/\partial P)_{T,P=0}$ without adjustment for the piezoelectric contribution. Both $(\partial C_{33}/\partial P)_{T,P=0}$ and $(\partial C_{44}/\partial P)_{T,P=0}$ increase approximately linearly with increasing temperature. Both $(\partial C_{13}/\partial P)_{T,P=0}$ and $(\partial B/\partial P)_{T,P=0}$ exhibit quite deep minima at about 333 K in their temperature dependences; these accrue from the measured value of $(1/W_0)(\partial W/\partial P)_{P=0}$ for mode 10, which shows a pronounced minimum at this temperature. The physical source of these minima is not yet known.

Knowledge of the compression $V(P)/V_0$ (the ratio of the volume $V(P)$ to the V_0 at atmospheric pressure) is useful in theoretical studies of the physical properties of a solid under pressure. Although the dependence of ultrasonic wave velocity upon pressure can be measured with precision, the pressure range is limited. To evaluate the compression at higher pressure, an extrapolation procedure based on the Murnaghan[25] equation of state

$$P=\frac{B_0^T}{B_0'^T}\left[\left[\frac{V_0}{V(P)}\right]^{B_0'^T}-1\right], \tag{11}$$

can be used in the form

$$\ln\left[\frac{V_0}{V(P)}\right]=\frac{1}{B_0'^T}\ln\left[B_0'^T\left[\frac{P}{B_0^T}\right]+1\right]. \tag{12}$$

TABLE IV. Comparison between $(1/W_0)(\partial W/\partial P)_{T,P=0}$ measured for VHPQ at 298 K and the previous data for quartz (Ref. 10). Units are 10^{-11} Pa^{-1}.

Mode	Data (VHPQ)	Ref. 10	Mode	Data (VHPQ)	Ref. 10
1	2.173±0.022	1.511	7	4.386±0.025	4.507
2	0.388±0.004	0.466	9	1.631±0.016	(mode 8) 1.671
5	5.085±0.051	3.956	10	5.061±0.051[a]	2.190
6	−3.467±0.035	−3.665	12	2.818±0.028[a]	

[a]Measured on left-handed quartz. In mode 12, the wave propagation direction is along $[0\ -1/\sqrt{2}\ 1/\sqrt{2}]$ and the polarization direction is along [100].

This describes the compression of many solids well.[26] Ultrasonic measurements give adiabatic moduli, so to use this equation of state it is necessary to transform the input data to isothermal moduli. The adiabatic bulk modulus B_0^S for α-quartz obtained at 298 K from

$$B_0^S=[(C_{11}+C_{12})C_{33}-2C_{13}^2]/[(C_{11}+C_{12})+2C_{33}-4C_{13}] \quad (13)$$

is given in Table I and its pressure derivative $(\partial B/\partial P)_{T,P=0}$ written as $(B_0'^S)$ at 298 K, from

TABLE V. (a) The hydrostatic-pressure derivatives $(\partial C_{IJ}/\partial P)_{T,P=0}$ of the elastic-stiffness-tensor components including (indicated by "*i*") and not including (indicated by "*n*") the piezoelectric contribution $(\partial e_i/\partial P)_{T,P=0}$ of VHPQ determined between 243 and 393 K and the comparison with previous data at 298 K. (b) The hydrostatic-pressure derivatives $(\partial C_{IJ}/\partial P)_{T,P=0}$ for those elastic-stiffness-tensor components that do not involve a piezoelectric contribution, the hydrostatic-pressure derivatives $(\partial B/\partial P)_{T,P=0}$ of the adiabatic bulk modulus, and $(\partial e_i/\partial P)_{T,P=0}$ of α-quartz between 243 and 393 K and the comparison with previous data at 298 K.

(a)

	$(\partial C_{11}/\partial P)_{T,P=0}$		$(\partial C_{12}/\partial P)_{T,P=0}$		$(\partial C_{13}/\partial P)_{T,P=0}$		$(\partial C_{66}/\partial P)_{T,P=0}$	
	i	*n*	*i*	*n*	*i*	*n*	*i*	*n*
T (K)	±0.04	±0.02	±0.05	±0.06	±0.02	±0.02	±0.03	±0.05
243	3.43	1.89	9.70	11.23	6.83	7.30	−3.13	−4.67
253	3.50	1.69	9.82	11.63	5.95	6.49	−3.16	−4.97
263	3.54	1.44	9.95	12.05	5.24	5.87	−3.21	−5.31
273	3.64	1.36	10.14	12.42	4.20	4.89	−3.25	−5.53
283	3.73	1.15	10.13	12.72	3.43	4.20	−3.20	−5.78
293	3.78	1.17	9.86	12.47	3.25	4.03	−3.04	−5.65
298	3.81	1.49	9.80	12.12	3.34	4.04	−2.99	−5.32
303	3.79	1.44	9.65	12.00	2.95	3.65	−2.93	−5.28
313	3.89	1.91	9.67	11.65	2.79	3.39	−2.89	−4.87
323	3.94	2.21	9.77	11.50	1.42	1.94	−2.91	−4.64
333	3.95	2.28	10.05	11.71	0.34	0.84	−3.05	−4.71
343	3.97	3.09	10.27	11.15	0.93	1.19	−3.15	−4.03
353	4.06	3.66	10.57	10.97	1.69	1.81	−3.26	−3.65
363	4.12	4.09	10.85	10.88	3.00	3.01	−3.37	−3.40
373	4.11	4.50	11.12	10.72	4.30	4.18	−3.51	−3.11
383	4.09	4.93	11.34	10.50	5.79	5.54	−3.63	−2.79
393	4.08	5.58	11.44	9.93	7.01	6.56	−3.68	−2.18
298[a]	3.28		8.66		5.97		−2.69	

(b)

T (K)	$(\partial C_{33}/\partial P)_{T,P=0}$ ±0.03	$(\partial C_{44}/\partial P)_{T,P=0}$ ±0.02	$(\partial C_{14}/\partial P)_{T,P=0}$ ±0.04	$(\partial B/\partial P)_{T,P=0}$ ±0.02	$(\partial e_1/\partial P)_{T,P=0}$ ±0.02	$(\partial e_2/\partial P)_{T,P=0}$ ±0.01
243	8.71	1.28	−3.86	7.00	1.54	−0.35
253	8.86	1.38	−4.06	6.75	1.81	−0.48
263	8.91	1.43	−4.29	6.55	2.10	−0.48
273	9.02	1.57	−4.37	6.26	2.28	−0.51
283	9.24	1.68	−4.46	6.04	2.58	−0.60
293	9.45	1.75	−4.27	5.92	2.61	−0.49
298	9.51	1.84	−3.96	5.92	2.32	−0.37
303	9.57	1.88	−3.91	5.73	2.35	−0.41
313	9.71	1.90	−3.52	5.67	1.98	−0.22
323	9.86	1.98	−3.29	5.17	1.73	−0.19
333	10.04	2.04	−3.29	4.84	1.66	−0.25
343	10.17	2.12	−2.69	5.05	0.87	−0.09
353	10.20	2.20	−2.34	5.40	0.39	−0.06
363	10.33	2.31	−2.07	5.95	0.03	−0.02
373	10.45	2.39	−1.74	6.48	−0.40	−0.00
383	10.56	2.41	−1.39	7.07	−0.84	0.14
393	20.77	2.51	−0.85	7.50	−1.50	0.42
298[a]	10.84	2.66	1.93	6.3	0.005	

[a]Reference 10.

$$B_0'^S=[(C_{11}+C_{12})C'_{33}+C_{33}(C'_{11}+C'_{12})-4C_{13}C'_{13}-B_0^S(C'_{11}+C'_{12})+2C'_{33}-4C'_{13}]/[(C_{11}+C_{12})+2C_{33}-4C_{13}]\ , \tag{14}$$

is listed in Table V(b). The adiabatic and isothermal bulk moduli are related by

$$B_0^S=B^T(1+\alpha\gamma T)\ . \tag{15}$$

For α-quartz, the thermal-expansion-tensor components obtained at 298 K by using the results given by McSkimin, Andreatch, and Thurston[10] are $\alpha_{11}=13.932\times10^{-6}$ K^{-1}, $\alpha_{33}=7.308\times10^{-6}$ K^{-1} so that the coefficient α of volume expansion is 35.172×10^{-6} K^{-1}. The Grüneisen parameter γ used in these calculations is 0.6544, which has been calculated from

$$\gamma=\frac{\alpha B_0^S}{\rho_0 C_P}\ , \tag{16}$$

where ρ_0 is the density of the VHPQ under atmospheric pressure and C_P is the heat capacity at constant pressure. A value for C_P of 740.9 $Jkg^{-1}K^{-1}$, estimated from the empirical equation given by Samsonov,[27] has been used. The calculated isothermal bulk modulus B_0^T of the VHPQ at room temperature is 3.626×10^{10} Pa. The hydrostatic pressure derivative $B_0'^T$ is given by[26,28]

$$B_0'^T=B_0'^S+T\alpha\gamma\frac{B_0^T}{B_0^S}\left[1-\frac{2}{\alpha B_0^T}\left[\frac{\partial B_0^T}{\partial T}\right]_P-2B_0'^S\right]+\left[T\alpha\gamma\frac{B^T}{B_0^S}\right]^2\left[B_0'^S-1-\frac{1}{\alpha^2}\left[\frac{\partial\alpha}{\partial T}\right]_P\right]\ , \tag{17}$$

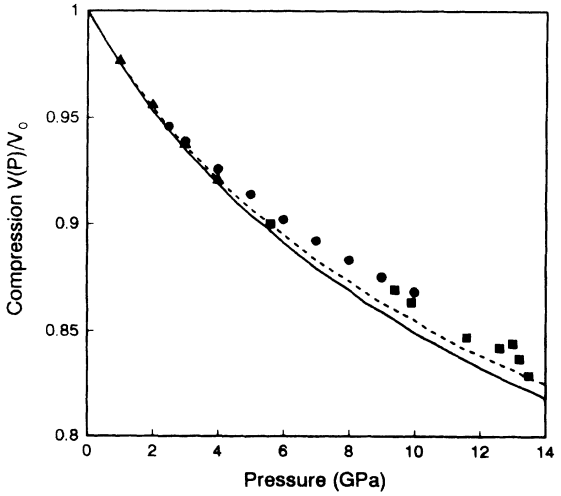

FIG. 1. The isothermal compression of quartz extrapolated to very high pressures (solid line) by using the Murnaghan equation of state in comparison with experimental data [filled triangles (Ref. 29), filled circles (Ref. 30), and filled squares (Ref. 31)]. The dotted line is the compression determined by Anderson (Ref. 26) using SOEC's and pressure derivative data from Ref. 10.

where $(\partial B_0^T/\partial T)_P$ can be obtained from

$$\left[\frac{\partial B_0^T}{\partial T}\right]_P=\frac{\partial B_0^S}{\partial T}\frac{1}{1+T\alpha\gamma}-\frac{B_0^S}{T}\frac{T\alpha\gamma}{(1+T\alpha\gamma)^2}\left[1+\frac{(\partial\alpha/\partial T)_P}{\alpha/T}\right]\ . \tag{18}$$

The temperature dependence of the adiabatic bulk modulus $(\partial B_0^S/\partial T)$, calculated from the measured elastic constants is -0.78×10^7 Pa K^{-1} for the VHPQ at 298 K. For VHPQ $(\partial\alpha/\partial T)_{T=298\text{ K}}$ is not yet known and so it has been estimated (as 6.604×10^{-8} K^{-1}) from the thermal-expansion coefficient results of McSkimin, Andreatch, and Thurston.[10] Insertion of data for B_0^S (Table I), α, γ, and $(\partial\alpha/\partial T)$ into Eq. (18) gives a value of $(\partial B_0^S/\partial T)_{T=298\text{ K}}$ of -9.04×10^6 Pa K^{-1}, and then from Eq. (17) $B_0'^T$ $(=\partial B_0^T/\partial P)$ is 5.94. The compression of the VHPQ, calculated using the Murnaghan equation of state,[12] is compared with that of natural quartz calculated by Anderson[26] who used the data measured by McSkimin, Andreatch, and Thurston[10] and with those measured by Bridgman[29,30] and Wackerle[31] (Fig. 1). At high pressures the experimentally determined compression is rather less than that estimated from the ultrasonic data as would be expected due to the tendency in any material towards an increased stiffness in this pressure regime.

IV. THE ELASTIC-STIFFNESS TENSOR COMPONENTS AND THEIR HYDROSTATIC-PRESSURE DERIVATIVES CALCULATED USING THE ATOMISTIC SIMULATION METHOD (ASM)

Atomistic simulation is an effective technique for predicting structural, elastic and thermodynamic properties of solids. The approach adopted in this study is based on the classical Born model of solids, in which potential energy functions represent the interactions between pairs or groups of ions or atoms in the structure. This representation allows a range of properties to be determined, including the vibrational characteristics of a crystal. The sum of interaction energies gives the lattice energy of the crystal. In general the potential model used to describe the interaction between a pair of ions is given by a simple analytical expression

$$V_{ij}(r_{ij})=\frac{q_iq_j}{r_{ij}}+A_{ij}\exp\left[-\frac{r_{ij}}{\rho_{ij}}\right]-\frac{C_{ij}}{r_{ij}^6}\ , \tag{19}$$

where the first term is the long-range electrostatic interaction, q_i and q_j being the charges of the ions i and j, separated by a distance r_{ij}. The second and third terms correspond to the short-range interaction, where the parameters A_{ij}, ρ_{ij}, and C_{ij} are required for every pair of species. The exponential term represents the repulsive

Table VI. Potential parameters used in the atomistic simulation.

Interaction	A (eV)	ρ_{ij} (Å^{-1})	C_{ij} (eV Å^6)	Atomic charges
O-O	1388.7730	2.7600	175.0000	$q_O = -1.2$
Si-O	18003.7572	4.8731	133.5381	$q_{Si} = 2.4$

component between neighboring charge clouds and the last term models the dispersive interactions. The accuracy of an atomic simulation method depends almost entirely upon the chosen potential. The SOEC's are second derivatives of the lattice energy with respect to strain and their calculation provides a rigorous test of the potential used. An even more stringent demand on the model is to reproduce the experimental values of the hydrostatic-pressure derivatives of the SOEC's which are third derivatives of the lattice energy.

The potential used in this work was derived quantum mechanically.[32] In this calculation, the Si and O ions were treated as rigid and assigned partial charges, +2.4 for Si ions and −1.2 for O ions. The potential parameters used in the modelling are listed in Table VI. To perform the calculation, the computer code PARAPOCS (Ref. 33) has been used to find the minimum energy structure at a specific pressure and temperature. This method is based on lattice dynamics and calculates vibrational frequencies in periodic structures. A major assumption of these calculations is the quasiharmonic approximation, which assumes that the vibrational motions in the solid are comprised of independent quantized harmonic oscillators whose frequencies vary with the cell volume.

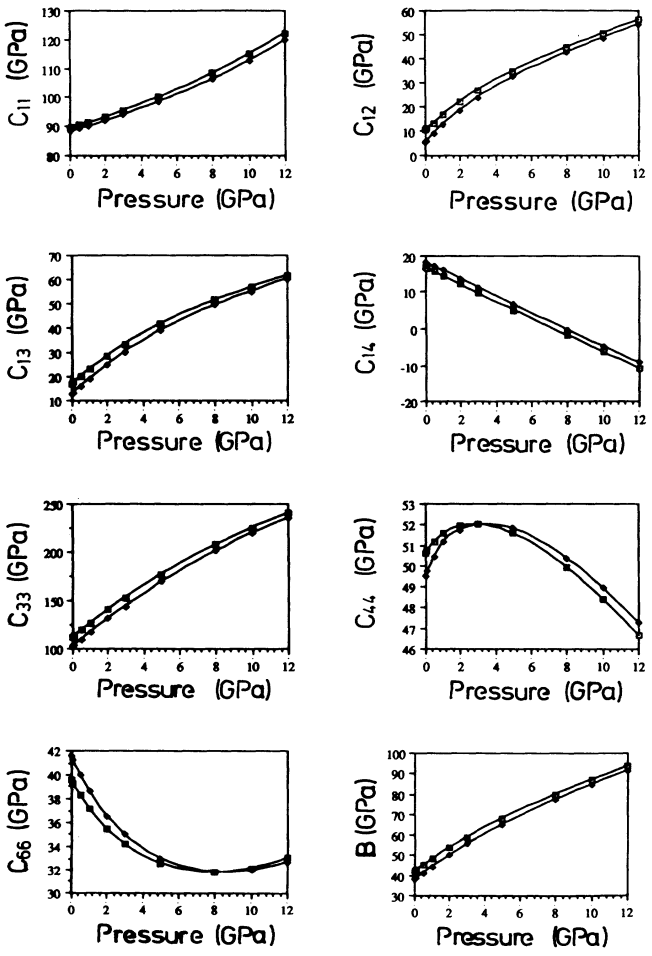

FIG. 2. The pressure dependences of the elastic-stiffness-tensor components C_{IJ} of quartz at 0 K (squares) and 300 K (diamonds) calculated using the atomistic simulation method.

The pressure dependences of the SOEC's and the bulk modulus of α-quartz have been calculated from zero pressure to 12 GPa at 0 and 300 K, respectively. The calculated SOEC's at zero pressure are in good agreement with the measured quantities (Table I). The calculated results show nonlinear dependences of the SOEC's on pressure (Fig. 2). Interestingly C_{44} reaches a maximum at about 30×10^8 Pa, while C_{66} has a minimum around 80×10^8 Pa. The pressure derivatives of the SOEC's as $P\rightarrow0$ have been obtained by a least-square fit method applied to the data from zero pressure to 0.5 GPa. In view of the complexity of quartz the calculated and measured hydrostatic-pressure derivatives of the elastic-stiffness-tensor components (Table VII) are in good agreement validating the theoretical potential. In particular the theoretical and measured values of $(\partial C_{11}/\partial P)_{T,P=0}$ and $(\partial C_{44}/\partial P)_{T,P=0}$ agree well. Both the measured and theoretically calculated pressure derivatives of the bulk modulus are close to each other. All of the $(\partial C_{IJ}/\partial P)_{T,P=0}$ are positive except for the $(\partial C_{66}/\partial P)_{T,P=0}$ and $(\partial C_{14}/\partial P)_{T,P=0}$. Thus, the theoretical calculation confirms the experimental finding of a negative value for $(\partial C_{14}/\partial P)_{T,P=0}$ for VHPQ. The $(\partial C_{IJ}/\partial P)_{T,P=0}$ obtained from the theoretical calculation do not show as large a change between 0 and 300 K (Table VII) as the measured temperature dependences between 243 and 393 K (Table V).

V. THE NEGATIVE PRESSURE DERIVATIVES OF SOEC AND THE α-β PHASE TRANSITION

α-quartz (space group $P3_221$ or $P3_121$ corresponding to handedness) transforms[34] at 846 K to β-quartz (space group $P6_422$ or $P6_222$). In the high-temperature structure each Si atom is sited almost in the same position as in α-quartz. The transition is driven by an optic phonon,[35] which is very soft in the [ξ00] direction. There is only one irreducible representation for phonons in α-quartz with $\mathbf{q}$ in the [ξ00] direction so that one branch cannot cross another: as the optic branch softens it

TABLE VII. Comparison between the theoretical values of the hydrostatic-pressure derivatives $(\partial C_{IJ}/\partial P)_{T,P=0}$ of the elastic-stiffness-tensor components of α-quartz determined using the ASM model and those measured experimentally.

T (K)	$(\partial C_{11}/\partial P)_{T,P=0}$	$(\partial C_{12}/\partial P)_{T,P=0}$	$(\partial C_{13}/\partial P)_{T,P=0}$	$(\partial C_{66}/\partial P)_{T,P=0}$
0	1.72±0.01	6.79±0.03	6.31±0.02	−2.53±0.02
300	1.41±0.02	7.89±0.05	6.91±0.03	−3.24±0.03
298[a]	1.49±0.02	12.12±0.05	4.04±0.04	−5.32±0.05
T (K)	$(\partial C_{14}/\partial P)_{T,P=0}$	$(\partial C_{33}/\partial P)_{T,P=0}$	$(\partial C_{44}/\partial P)_{T,P=0}$	$(\partial B/\partial P)_{T,P=0}$
0	−2.22±0.01	14.72±0.02	1.10±0.02	6.33±0.01
300	−1.98±0.01	15.39±0.03	1.75±0.03	6.85±0.02
298[a]	−3.96±0.04	9.51±0.03	1.84±0.02	5.92±0.02

[a]Measured data, not including the piezoelectric contributions $(\partial e_i/\partial P)_{T,P=0}$.

pushes the transverse-acoustic phonon in that direction down. This depressed acoustic branch has a slope ω/q equal to $(C_{66}/\rho)^{1/2}$. The experimental value of C_{66} for α-quartz is consistent with the calculated depression of this acoustic branch for a wave vector close to the zone center.[36] The shear elastic stiffness C_{66} for α-quartz shows an anomalous increase with temperature[21] and $(\partial C_{66}/\partial P)_T$ has a negative value, features that identify acoustic-mode softening.[37] A decrease in an elastic constant under the influence of pressure can indicate incipient lattice instability because it corresponds to a reduction in crystal stiffness for the associated acoustic-phonon mode. The finding of a negative pressure derivative for C_{66} indicates that even at room temperature there could be a degree of interaction between the soft optic phonon and the transverse-acoustic phonon in the same crystallographic direction leading to the anomalous behavior of C_{66} with pressure and temperature.

The main contribution to the strain at the α-β transition is produced by rotation of the SiO_4 tetrahedra about their respective twofold axes,[38] which comprises the displacement parameter in the α-quartz structure. The soft-phonon eigenvector involves 20% Si stretch, 70% oxygen tetrahedron rotation, and 10% oxygen stretch; displacements evinced not only by the anomalous behavior of C_{66} but also by that of C_{14}. The soft optic mode has B_1 symmetry.[39] There is no plane wave of B_1 symmetry in quartz: C_{14} is always coupled to other elastic constants. Höchli and Scott showed[38] that the soft elastic constant C_{14} in α-quartz is related to the displacement parameter x_0 by $C_{14}\sim x_0$ and ultrasonic measurements show that near the transition temperature the elastic constant $C_{14}(T)$ behaves as the displacement parameter, as does the soft optic phonon frequency $\omega(T)$. Therefore it can be deduced that the negative $(\partial C_{14}/\partial P)_T$ is also one of the results of the interaction between the soft optic phonon and the transverse-acoustic phonon in quartz.

VI. THE ACOUSTIC-MODE GRÜNEISEN PARAMETERS

The pressure derivatives of the SOEC's quantify the hydrostatic components of the coefficients of the cubic terms $(\partial^3 U(\eta)/\partial\eta_{ab}\partial\eta_{cd}\partial\eta_{ef})_{\eta=0}$ in the expansion of the strain energy density $U(\eta)$ with respect to the Lagrangian strain and thus, the leading term describing the vibrational anharmonicity of the long-wavelength acoustic phonon modes. Normal practice is to discuss vibrational anharmonicity in the quasiharmonic approximation in terms of mode Grüneisen parameters

$$\gamma(p,\mathbf{q}) = -(\partial \ln\omega(p,\mathbf{q})/\partial \ln V)_{T,P=0} . \tag{20}$$

Here $\omega(p,\mathbf{q})$ is the vibrational frequency of a mode of wavevector q. In the quasiharmonic approximation phonon frequencies change with temperature only through the lattice dimension, i.e., they are strain dependent and the generalized Grüneisen parameter can be calculated from the elastic constants and their pressure dependences.

For the particular case of volume change induced by an applied hydrostatic pressure P, Brugger[40] introduced a generalized Grüneisen parameter

$${}_H\gamma_p^T(\mathbf{q}) = \left[\frac{V}{\omega_p(\mathbf{q})} \left(\frac{\partial\omega_p(\mathbf{q})}{\partial V} \right)_T \right]_{P=0} . \tag{21}$$

For a piezoelectric crystal the mode Grüneisen parameter can be calculated using

$${}_H\gamma_p^T(\mathbf{N}) = -\frac{B^T}{2w_p(\mathbf{N})}[1+2s^T_{aajk}w_p(\mathbf{N})U_jU_k - B^{st}_{jrks}U_jU_kN_rN_s] . \tag{22}$$

Here B^{st}_{jrks} are the hydrostatic-pressure derivatives of the stiffened thermodynamic elastic stiffnesses. By considering the relationships between B^{st}_{jrks} and B_{jrks} and those between B_{jrks} and the pressure derivatives of the effective elastic

stiffnesses, one can obtain the equations required for calculating ${}_H\gamma_p^T(\mathbf{N})$ from the hydrostatic-pressure derivatives of the effective elastic stiffnesses and for piezoelectric crystals in Laue group RI these equations can be written as

$$
\begin{aligned}
{}_H\gamma_p^T(\mathbf{N}) = -\frac{B^T}{2w_p}\Bigg\{ & 2w_p[s_1(U_1^2+U_2^2)+s_3U_3^2] - \left[\left[\frac{\partial C_{11}}{\partial P}\right]_T + \left[\frac{\partial e_1}{\partial P}\right]_T + 1 + (2s_1-s_3)C_{11}^{S,E}\right](N_1U_1+N_2U_2)^2 \\
& - \left[\left[\frac{\partial C_{66}}{\partial P}\right]_T + \left[\frac{\partial e_1}{\partial P}\right]_T + 1 + (2s_1-s_3)C_{66}^{S,E}\right](N_1U_1-N_2U_2)^2 \\
& - \left[\left[\frac{\partial C_{33}}{\partial P}\right]_T + 1 + (3s_3-2s_1)C_{33}^{S,E}\right]N_3^2U_3^2 \\
& - \left[\left[\frac{\partial C_{44}}{\partial P}\right]_T + 1 + s_3C_{44}^{S,E}\right][(N_2U_3+N_3U_2)^2+(N_1U_3+N_3U_1)^2] \\
& - 2\left[\left[\frac{\partial C_{13}}{\partial P}\right]_T - 1 + s_3C_{13}^{S,E}\right][(N_1U_1+N_2U_2)N_3U_3] \\
& - 2\left[\left[\frac{\partial C_{14}}{\partial P}\right]_T + s_1C_{14}^{S,E}\right][(N_1^2-N_2^2)U_2U_3+(U_1^2-U_2^2)N_2N_3+2N_1U_1(N_2U_3+N_3U_2)]\Bigg\}\,, \qquad (23)
\end{aligned}
$$

where

$$
\begin{aligned}
w_p = {} & C_{11}^{S,E}(N_1U_1+N_2U_2)^2 + C_{66}^{S,E}(N_1U_2-N_2U_1)^2 + C_{33}^{S,E}N_3^2U_3^2 + C_{44}^{S,E}[(N_2U_3+N_3U_2)^2+(N_1U_3+N_3U_1)^2] \\
& + 2C_{13}^{S,E}(N_1N_3U_1U_3+N_2N_3U_2U_3) + 2C_{14}^{S,E}(N_1^2U_2U_3-N_2^2U_2U_3+N_2N_3U_1^2+2N_1N_2U_1U_3+2N_1N_3U_1U_2) \\
& + \frac{\{e_{11}[(N_1^2-N_2^2)U_1-2N_1N_2U_2]+e_{14}[N_2(N_1U_3-N_3U_1)+N_1(N_3U_2-N_2U_3)]\}^2}{[\varepsilon_{11}(N_1^2+N_2^2)+\varepsilon_{33}N_3^2]}\,, \qquad (24)
\end{aligned}
$$

and

$$s_1 = s_{11}^T + s_{12}^T + s_{13}^T\,, \qquad (25)$$

$$s_3 = 2s_{13}^T + s_{33}^T\,. \qquad (26)$$

The acoustic-mode Grüneisen parameters in the long wavelength limit have been calculated as a function of acoustic-mode propagation direction and temperature from the measured elastic constants and their pressure derivatives. Selected mode Grüneisen parameters as a function of sound wave propagation direction are given in Fig. 3 at 243 and 333 K. It can be seen that the values of the parameters are strongly dependent on the sound wave propagation direction as would be expected in a highly anisotropic crystal. An exception is γ_L in the *Y-Z* plane, which does not change much with propagation direction especially at higher temperatures. The substantial directional dependence of the acoustic-mode Grüneisen parameters is consistent with the anisotropy shown by the linear thermal-expansion coefficients. In the absence of mode softening the elastic constants and the lattice vibrational frequencies increase under hydrostatic pressure, which raises the strain-free energy, so that normally the mode Grüneisen gammas are positive. For quartz, most values of the mode Grüneisen gammas are positive and lie in the usual range up to about 2. However many mode gammas on one shear branch have negative values; these arise because $(\partial C_{66}/\partial P)_{T,P=0}$ is negative throughout the whole temperature range. There are substantial changes in γ_{s1} and γ_{s2} with sound wave propagation direction in the *Z-X* plane in the vicinity of 333 K as the temperature is changed. These correspond to the occurrence of the minima in $(\partial C_{13}/\partial P)_{T,P=0}$ and $(\partial B/\partial P)_{T,P=0}$ (Table V).

The temperature dependences of the acoustic-mode Grüneisen gammas of the modes propagated along the *X*, *Y*, and *Z* axes are shown in Fig. 4. The notations used to define the shear modes, which can be propagated along these three axes, are given in Table VIII. Most of these parameters show a marked temperature dependence. The influence of the negative value of $(\partial C_{66}/\partial P)_{T,P=0}$ can be seen in the findings that γ_{s2} for wave propagation along the *X* axis and γ_{s1} in *Y* axis have negative values ranging from -0.793 to -0.063 and -1.184 to -0.916, respectively.

In addition to being responsible for the nonlinear acoustic properties of a crystal under finite strain, the anharmonicity of lattice vibrations brings about thermal expansion. At a given temperature the expansion results from summation of the anharmonic effects of all the excited phonon modes rather than solely the acoustic modes at the long-wavelength limit so that the thermal Grüneisen parameter

$$\gamma^{\text{th}} = \frac{\alpha V B^T}{C_V} = \frac{\alpha V B^S}{C_P}\,, \qquad (27)$$

TABLE VIII. Terminology used to define shear acoustic-mode Grüneisen parameters along the three major crystallographic axes.

	X axis			*Y* axis			*Z* axis		
γ_P	U_1	U_2	U_3	U_1	U_2	U_3	U_1	U_2	U_3
γ_{s1}	0	β_2	$-\beta_1$	0	γ_1	γ_2	1	0	0
γ_{s2}	0	β_1	β_2	0	$-\gamma_2$	γ_1	0	1	0

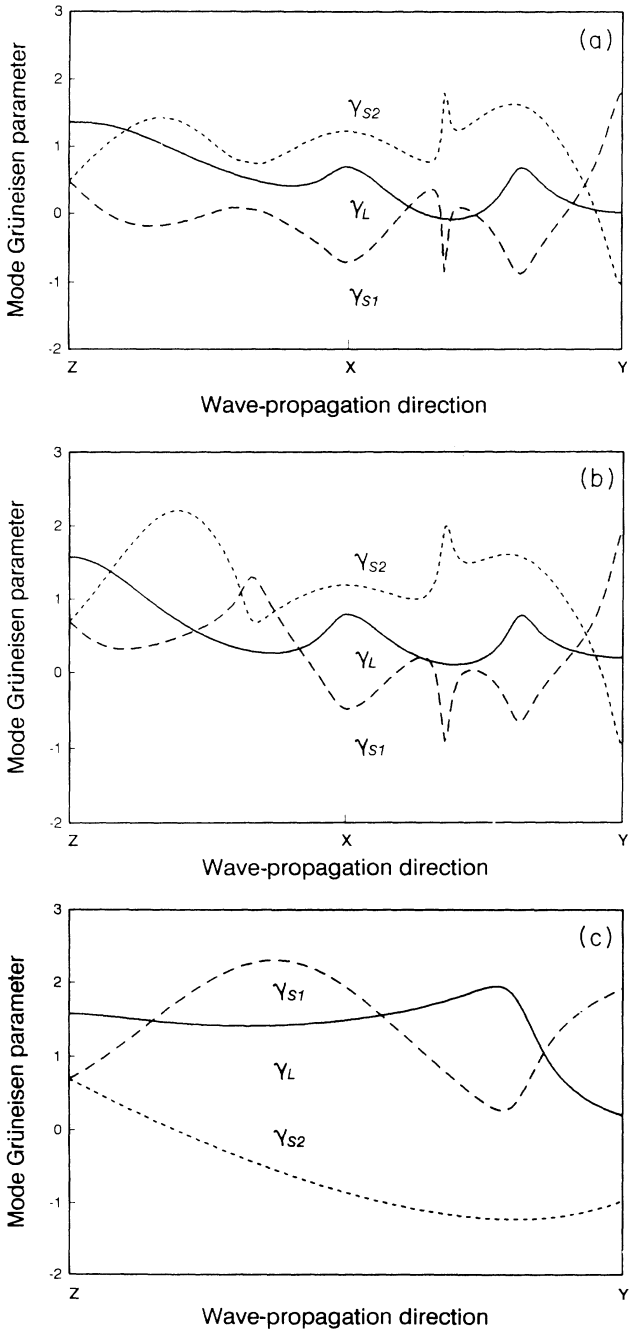

FIG. 3. The directional dependence of Grüneisen parameters for mode propagation in (a) the *Z*-*X* and *X*-*Y* planes at 243 K, (b) the *Z*-*X* and *X*-*Y* planes at 333 K, and (c) the *Y*-*Z* plane at 333 K.

(where α is the volume thermal expansion coefficient, B^T and B^S are the isothermal and isentropic bulk moduli, and C_V and C_P are the specific heat at constant volume and under constant pressure, respectively) can be expressed as the weighted average of mode Grüneisen parameters γ_i

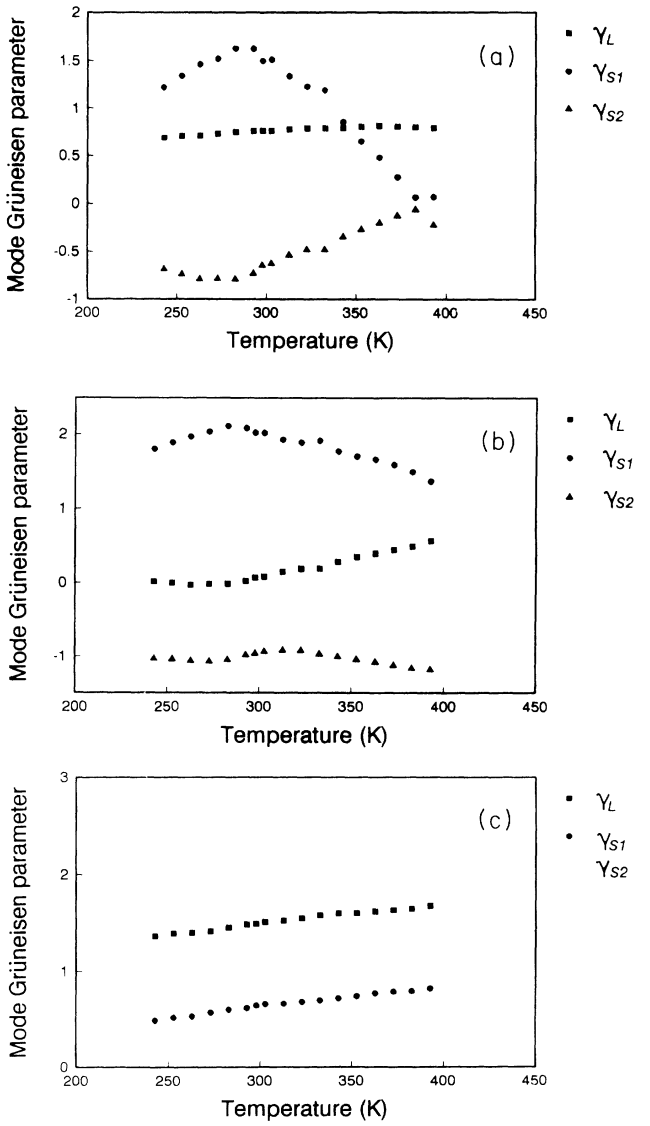

FIG. 4. The temperature dependences of the Grüneisen parameters of the modes propagated along (a) the *X*, (b) the *Y*, and (c) the *Z* axis.

$$\gamma^{\text{th}} = \frac{\sum_i \gamma_i c_i}{\sum_i c_i} \tag{28}$$

where c_i represents the Einstein heat capacity associated with a mode i and reflects the contribution of the ith mode to γ^{th}. The mean long-wavelength acoustic-mode Grüneisen parameter γ_H^{el} in the high-temperature limit (H) calculated using the elastic-stiffness-tensor and pressure derivative data, which include the piezoelectric contribution is plotted in Fig. 5. The observation that ($C_{11}/C_{33}=0.80$) (Table I) shows that elastically quartz is rather softer in the basal plane than in the direction of the threefold axis and the anisotropy ($\alpha_{33}<\alpha_{11}$) of the thermal-expansion-tensor components evinces this. Between 200 and 500 K, the thermal Grüneisen parameter γ^{th} of quartz reduces from about 0.75 to 0.64 (Fig. 5).[41] At these temperatures γ^{th} should be much influenced by optic mode contributions. Stress dependence measurements of Raman-active mode frequencies,[42,43] reveal that lower frequency optic modes have large positive Grüneisen parameters. At low temperature ($T \ll \Theta_D$) the thermal expansion is mainly dominated by the acoustic vibration modes, and the negative values of some of the acoustic-mode Grüneisen parameters (Fig. 4) cause the mean Grüneisen tensor component γ_{33} to decrease as the temperature is lowered until it, and the thermal-expansion-tensor component α_{33}, become negative.[41]

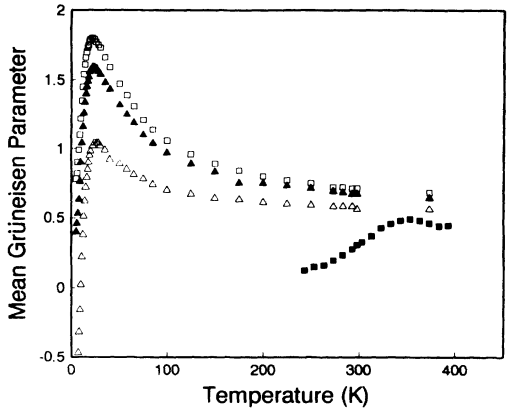

FIG. 5. The temperature dependence of the mean long-wavelength acoustic-mode Grüneisen parameter γ_H^{el} in the high-temperature limit (filled squares) for VHPQ and the thermal Grüneisen parameter γ^{th} (filled triangles) and its two tensor components γ_{11} (open squares) and γ_{33} (open triangles).[41]

ACKNOWLEDGMENTS

Many thanks are due to the ministry of Defence (United Kingdom), Defence Research Agency (Electronics Division), formerly the Royal Signals and Radar Establishment, without whose funding the experimental program would not have been possible

[1]I. Koga, M. Aruga, and Y. Yoshinaka, Phys. Rev. **109**, 1467 (1958).
[2]H. J. McSkimin, J. Acoust. Soc. Am. **34**, 1271 (1962).
[3]A. G. Ludanov, A. A. Fotchenkov, and L. A. Yakovlev, Akust. Zh. **22**, 612 (1976) [Sov. Phys. Acoust. **22**, 343 (1976)].
[4]M. M. Shevel'ko and L. A. Yakovlev, Akust. Zh. **23**, 331 (1977) [Sov. Phys. Acoust. **23**, 187 (1977)].
[5]J. C. Brice, Rev. Mod. Phys. **57**, 105 (1985).
[6]B. J. James, Ph.D. thesis, Royal Holloway and Bedford New College, University of London, 1987.
[7]R. Fowles, J. Geophys. Res. **72**, 5729 (1967).
[8]R. A. Graham, Phys. Rev. B **6**, 4779 (1972).
[9]R. N. Thurston, H. J. McSkimin, and P. Andreatch, J. Appl. Phys. **37**, 267 (1966).
[10]H. J. McSkimin, P. Andreatch, and R. N. Thurston, J. Appl. Phys. **36**, 1624 (1965).
[11]E. P. Papadakis, J. Acoust. Soc. Am. **42**, 1045 (1967).
[12]S. C. Flower and G. A. Saunders, Philos. Mag. B **62**, 311 (1990).
[13]H. J. McSkimin, J. Acoust. Soc. Am. **33**, 12 (1961).
[14]H. E. Altman and R. T. Beyer, J. Acoust. Soc. Am. **59**, 545 (1976).
[15]E. Kittinger, Ultrasonics **15**, 30 (1977).
[16]E. P. Papadakis, J. Acoust. Soc. Am. **40**, 863 (1966).
[17]G. F. Davies and R. J. O'Connell, in *High-Pressure Research Applications in Geophysics,* edited by M. H. Maghnani and S. I. Akimoto (Academic, New York, 1977).
[18]R. N. Thurston and K. Brugger, Phys. Rev. **133**, A1604 (1964).
[19]W. Voigt, *Lehrbuch der Kristallphysik,* 1st ed. (Teubner, Leipzig, 1910), p. 752.
[20]W. P. Mason, Bell Syst. Tech. J. **22**, 178 (1943).
[21]J. V. Atanasoff and P. J. Hart, Phys. Rev. **59**, 85 (1941).
[22]R. N. Thurston, Proc. IEEE **53**, 1320 (1965).
[23]R. N. Thurston, J. Acoust. Soc. Am. **37**, 348 (1965).
[24]*IEEE Standard on Piezoelectricity* (The Institute of Electrical and Electronic Engineers Inc., New York, 1978), Vol. 176.
[25]F. D. Murnaghan, Proc. Nat. Acad. Sci. USA **30**, 244 (1944).
[26]O. L. Anderson, J. Phys. Chem. Solids. **27**, 547 (1966).
[27]*The Oxide Handbook,* edited by G. V. Samsonav, translated by C. Nigel Turton and Tatiana I. Turton (IFI/Plenum, New York, 1973), p. 130.
[28]W. C. Overton, J. Chem. Phys. **37**, 116 (1962).
[29]P. W. Bridgman, Proc. Am. Acad. Arts Sci. **76**, 55 (1948).
[30]P. W. Bridgman, Proc. Am. Acad. Arts Sci. **76**, 71 (1948).
[31]J. Wackerle, J. Appl. Phys. **33**, 922 (1962).
[32]B. W. H. van Beest, G. J. Kramer, and R. A. van Santen, Phys. Rev. Lett. **64**, 1955 (1990).
[33]S. C. Parker and G. D. Price, Adv. Solid State Chem. **1**, 295 (1989).
[34]C. R. LeChatelier, Acad. Sci. (Paris, 1889).
[35]J. D. Axe and G. Shirane, Phys. Rev. B **1**, 342 (1970).
[36]K. H. W. Bauer, H. Jagodzinski, B. Dorner, and H. Grimm, Phys. Status Solidi (B) **48**, 437 (1971).
[37]H. A. A. Sidek, G. A. Saunders, Wang Hong, Xu Bin, and Han Jianru, Phys. Rev. B **36**, 7612 (1987).

[38]U. T. Höchli and J. F. Scott, Phys. Rev. Lett. **26**, 1627 (1971).
[39]S. M. Shapiro, D. C. O'Shea, and H. Z. Cummins, Phys. Rev. Lett. **19**, 361 (1967).
[40]K. Brugger, Phys. Rev. **137**, A1826 (1965).
[41]T. H. K. Barron, J. F. Collins, T. W. Smith, and G. K. White, J. Phys. C **15**, 4311 (1982).
[42]V. J. Tekippe, A. K. Ramdas, and S. Rodriguez, Phys. Rev. B **8**, 706 (1973).
[43]M. H. Grimsditch, A. K. Ramdas, S. Rodriguez, and V. J. Tekippe, Phys. Rev. B **15**, 5869 (1977).